Identifiability analysis and noninvasive online estimation of the first-order neural activation dynamics in the brain with transcranial magnetic stimulation

S.M.Mahdi Alavi[a,*], Adam Mahdi[b,c], Fidel Vila-Rodriguez[a], Stefan M. Goetz[d,e,f,g]

[a] *Department of Psychiatry, University of British Columbia, Vancouver, BC, Canada*
[b] *Surrey Institute for People-centred Artificial Intelligence, University of Surrey, Surrey, UK*
[c] *Oxford Internet Institute, University of Oxford, Oxford, UK*
[d] *Department of Engineering, University of Cambridge, Cambridge, UK*
[e] *Department of Psychiatry and Behavioral Sciences, Duke University, Durham, NC, USA*
[f] *Department of Electrical and Computer Engineering, Duke University, Durham, NC, USA*
[g] *Department of Neurosurgery, Duke University, Durham, NC, USA*

Abstract

Background: Neurons demonstrate very distinct nonlinear activation dynamics, influenced by the neuron type, morphology, ion channel expression, and various other factors. The measurement of the activation dynamics can identify the neural target of stimulation and detect deviations, e.g., for diagnosis. This paper describes a tool for closed-loop sequential parameter estimation (SPE) of the activation dynamics through transcranial magnetic stimulation (TMS). The proposed SPE method operates in real time, selects ideal stimulus parameters, detects and processes the response, and concurrently estimates the input–output (IO) curve and the first-order approximation of the activated neural target.
Objective: To develop a SPE method to concurrently estimate the first-order activation dynamics and IO curve in closed-loop electromyography-guided (EMG-guided) TMS.
Method: First, identifiability of the integrated model of the first-order neural activation dynamics and IO curve is assessed, demonstrating that at least two IO curves need to be acquired with different pulse widths. Then, a two-stage SPE method is proposed. It estimates the IO curve by using Fisher information matrix optimization in the first stage and subsequently estimates the membrane time constant as well as the coupling gain in the second stage. The procedure continues in a sequential manner until a stopping rule is satisfied.
Results: The results of 73 simulation cases confirm the satisfactory estimation of the membrane time constant and coupling gain with average absolute relative errors (AREs) of 6.2% and 5.3%, respectively, with an average of 344 pulses (172 pulses for each IO curve or pulse width). The method estimates the IO curves' lower and upper plateaus, mid-point, and slope with average AREs of 0.2%, 0.7%, 0.9%, and 14.5%, respectively.
Conclusions: SPE of the activation dynamics requires acquiring at least two IO curves with different pulse widths, which needs a TMS device with adjustable pulse duration.
Significance: The proposed SPE method enhances the cTMS functionality, which can contribute novel insights in TMS studies.

Keywords: Controllable transcranial magnetic stimulation (cTMS), closed-loop EMG-guided TMS, neural membrane dynamics, input–output (IO) curve, estimation

1. Introduction

Transcranial magnetic stimulation is a noninvasive method for activating neurons in the brain [1, 2]. It has been approved for diagnosis as well as various therapeutic applications and has become an essential tool in experimental brain research [3]. Most of these applications desire a high stimulation selectivity to activate specific circuits [4]. While the achievable coil focality has physical limits [5], modifications of the pulse shape were found to address differences in the activation dynamics of various neuron populations for stimulation specificity [6, 7, 8, 9, 10, 11, 12, 13].

Changing the pulse shape does not only allow shifting the activation between different neural elements but also the analysis of the activation dynamics of the stimulated neural target [14, 15, 16, 17]. Although the neuron activation dynamics is highly nonlinear and therefore complicated to measure, a linear first-order approximation can already disclose differences between targets [10]. As this first-order linearization typically converges to a low-pass filter, the key parameters that can be extracted in such system identification are the time constant and the

*Corresponding Author
[1] E-mails: mahdi.alavi.work@gmail.com, adam.mahdi@oii.ox.ac.uk, fidel.vilarodriguez@ubc.ca, smg84@cam.ac.uk

static gain, also called coupling gain or coupling factor here [17, 18]. In addition to identifying and differentiating various stimulation targets, the activation dynamics of neurons are furthermore very sensitive to the environment of the neuron, genetic deviations, and diseases. Therefore, it is studied and tested for diagnostic purposes [19, 20, 21, 22, 23, 24, 25, 26, 27].

The approximate identification of the activation dynamics through the measurement of the time constant of the activated neural elements is typically performed in targets with readily detectable response, such as the primary motor cortex or rarer the visual cortex [6, 7, 28, 29]. In the primary motor cortex, strong stimulation pulses lead to muscle contraction in the periphery, which can be detected as motor evoked potentials (MEP), with latest methods even below the noise floor of background activity in electromyographic (EMG) recordings [30, 31, 32, 33].

Conventionally, the time constant is estimated off-line, which requires stimulation at various pulse widths and detection of the motor thresholds. Real-time estimation of the neural time constant and the coupling factor is a major challenging issue and requires closed-loop stimulation, analysis of the response, and decision about the parameters of the subsequent stimulus [18]. Furthermore, various technologies to change the pulse shape with a sufficiently wide range during operation have been proposed and developed to enable such closed-loop estimation of the time constant [34, 35, 36, 37, 38, 39].

Closed-loop TMS refers to the automatic and real-time adjustment of TMS parameters based on measurements, e.g., to maximize the desired plastic effects by using the brain/neural data in a feedback system or to speed up the detection of a biomarker [40, 41]. Among the simplest closed-loop TMS procedures are motor threshold estimation methods [42, 43, 44]. Closed-loop TMS is an area of active research using both EEG- [41, 45, 46, 47, 48] and EMG-guided TMS [18, 49, 50].

We previously proposed to use real-time parameter estimation of the neural membrane time constant and recruitment input–output (IO) curve and developed the necessary analytical relationships for a fixed coupling gain and TMS [18]. In sequential parameter estimation (SPE), a number of TMS pulses is administered, the estimation is updated after each stimulus, and the estimation continues until satisfying a stopping rule based on the the convergence of the model parameters [49]. The coupling gain depends on the neurostimulation technology including the coil, the geometric conditions, for instance, coil-to-cortex distance, head size, and neural population type as well as orientation relative to the induced electric field in transcranial magnetic stimulation (TMS) [17, 51].

As the key objective, this paper presents a tool for concurrent sequential parameter estimation of the membrane time constant and IO curve parameters including the coupling gain in closed-loop EMG-guided TMS. To achieve this goal, an integrated model of the full first-order neural membrane dynamics and IO curve is firstly developed. The identifiability analysis demonstrates that at least two IO curves with different pulse widths are required for concurrent sequential parameter estimation of the membrane time constant and coupling gain. This emphasizes the need for controllable TMS (cTMS) devices with adjustable pulse width. Then, we propose a two-stage sequential parameter estimation method which estimates the IO curve in the first stage and the membrane time constant as well as the coupling gain in the second stage. The IO curve is estimated by optimizing the Fisher information matrix [49]. The proposed method enhances the methodology and functionality of TMS and promises novel insights in the physiology and clinical applications.

The contributions of this paper are highlighted as follows:

- Formal identifiability analysis of the integrated model of the full first-order neural membrane dynamics and IO curve, which underlines that at least two IO curves at different pulse widths need to be acquired for concurrent sequential parameter estimation of the membrane time constant and coupling gain.

- Concurrent sequential parameter estimation of a full first-order dynamical model of the neural membrane (including the time constant and coupling gain) and pulse-width-dependent IO curve in closed-loop EMG-guided TMS.

2. Neural system model

Fig. 1 shows the overall structure of the neural system model, from the TMS pulse w to the MEP size y. The MEP size can be represented by various metrics, such as peak-to-peak voltage, area, or similar features [32]. $h(t)$ represents the dynamics of the neural membrane. This paper focuses on the first-order linear approximation model with the impulse-response function

$$h(t) = \frac{g}{\tau} e^{-t/\tau}, \tag{1}$$

where τ is the membrane time constant and g is the coupling gain between the TMS coil and the directly stimulated neurons, which can depend on factors such as the coil including shape and number of turns, coil-to-cortex distance and specific coil position, anatomy, properties of the neurons in the focus, including morphology and ion-channel expression, and orientation relative to the induced electric field [17, 52].

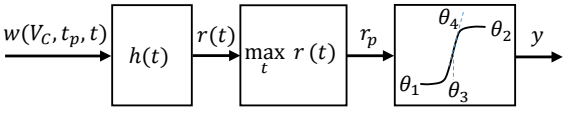

Figure 1: The overall structure of the neural system model, from the TMS pulse w to the MEP size y.

$r(t)$ denotes the membrane response to the stimulus w. Any TMS technology that can vary the pulse duration sufficiently can serve for this time-constant determination. Without loss of generality, this paper uses the original cTMS design [35] as an example, with

$$w(t) = \begin{cases} \delta \frac{V_C}{L} \Big(\cos \omega t - \frac{\sigma}{\omega} \sin \omega t \Big) e^{-\sigma t} & \text{if } t \le t_p, \\ -\delta \frac{V_C (R+r) \sin \omega t_p}{\omega L^2} e^{-\frac{(t-t_p)(R+r)}{L} - \sigma t_p} & \text{if } t > t_p, \end{cases} \tag{2}$$

where V_C is the normalized pulse voltage amplitude, adjustable between $V_C(\min) = 0$ and $V_C(\max) = 1$. t_p is the pulse width, which is assumed to be adjustable between $t_p(\min) = 10$ µs and $t_p(\max) = 200$ µs. Other parameters include the stimulating coil L, the energy dissipation resistor R of the free-wheeling path that generates the decay of the second pulse phase, the resistor r which represents the combined resistance of the capacitor, semiconductor switch, cables, and stimulation coil. Following the original cTMS design, the following parameter values are used in this paper: $L = 16$ µH, $C = 716$ µF, $R = 0.1$ Ω, $r = 20$ mΩ, $\delta = 3.2 \times 10^{-6}$ (V/m)(A/s). The parameters ω and σ are defined as

$$\omega = \sqrt{\frac{1}{LC} - \Big(\frac{r}{2L}\Big)^2}, \text{ and } \sigma = \frac{r}{2L}.$$

The parameter δ is a proportionality coefficient.

The stimulus response $r(t)$ is obtained by the convolution of w and h [18] and results in

$$r(t) = \begin{cases} \frac{k_1 g V_C}{\alpha\tau^2 - 2\sigma\tau + 1} \Big[-\omega e^{-t/\tau} + \\ \quad \Big((\alpha\tau - \sigma) \sin \omega t + \omega \cos \omega t \Big) e^{-\sigma t} \Big] & \text{if } t \le t_p \\ r(t_p) e^{-(t-t_p)/\tau} + \Big(e^{-(t-t_p)/\tau - t_p \sigma} \\ \quad - e^{-(t-t_p)(R+r)/L - t_p \sigma} \Big) k_2 g V_C & \text{if } t > t_p \end{cases} \tag{3}$$

where $r(t_p)$ is the neural membrane response at time $t = t_p$, and

$$\alpha = \omega^2 + \sigma^2, \; k_1 = \frac{\delta}{L\omega}, \; k_2 = \frac{k_1 (R+r) \sin \omega t_p}{\tau L (1/\tau - (R+r)/L)}.$$

We define the depolarization factor as the peak of r as

$$\begin{aligned} r_p(t^*, \tau, g) &= \max_{t=t^*} \; r(t) \\ &= \frac{k_1 g V_C}{\alpha\tau^2 - 2\sigma\tau + 1} \Big[-\omega e^{-t^*/\tau} + \\ &\quad \Big((\alpha\tau - \sigma) \sin \omega t^* + \omega \cos \omega t^* \Big) e^{-\sigma t^*} \Big] \end{aligned} \tag{4}$$

where t^* is the peak time.

An MEP is generated when the depolarization factor r_p reaches a certain threshold. Thus, the relationship between the depolarization factor and the MEP is modeled as a sigmoid function

$$y = y^h + \frac{y^l - y^h}{1 + \Big(r_p\Big)^s}, \tag{5}$$

where y is the MEP size and y^l as well as y^h represent the lower and upper plateaus of the IO curve.

By defining the parameter vector

$$\boldsymbol{\theta} = [\; \theta_1 \quad \theta_2 \quad \theta_3 \quad \theta_4 \;] = [\; y^l \quad y^h \quad \frac{V_C}{r_p(t^*, \tau, g)} \quad s \;], \tag{6}$$

an integrated model of the TMS neural system is obtained as

$$y = \theta_2 + \frac{\theta_1 - \theta_2}{1 + \Big(\frac{V_C}{\theta_3}\Big)^{\theta_4}}. \tag{7}$$

The mid point and slope of the IO curve are given by θ_3 and θ_4, respectively.

Fig. 2 presents a sample cTMS pulse $w(t)$, the first-order linear neural response $r(t)$, and the depolarization factor r_p.

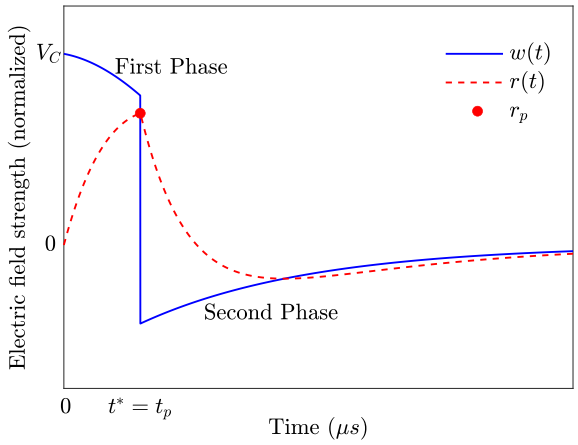

Figure 2: Sample cTMS pulse $w(t)$, first-order linear neural response $r(t)$, and depolarization factor r_p.

3. Problem Statement

The problem is to estimate the integrated model parameters, i.e., neural membrane time constant τ, gain g, and the IO curve parameters θ_i, $i = 1, \ldots, 4$ in a closed-loop system. Most importantly, all those parameters need to be estimated concurrently. This paper will discuss the identifiability conditions for such a concurrent estimation to subsequently provide a method.

4. Identifiability analysis

The proposed method is based on a two-stage sequential parameter estimation technique, where the estimation of the parameter vector $\boldsymbol{\theta}$ is firstly updated after each stimulus. Then, the estimation of the membrane time constant

and the coupling gain are updated by using the relationship between the IO curve's mid-point θ_3 and these parameters as follows:

$$\theta_3 = \frac{V_C}{r_p(t^*,\tau,g)} = \frac{\alpha\tau^2 - 2\sigma\tau + 1}{gk_1} \times \frac{1}{-\omega e^{-t^*/\tau} + \Big((\alpha\tau - \sigma)\sin\omega t^* + \omega\cos\omega t^*\Big)e^{-\sigma t^*}} \tag{8}$$

Be reminded that t^* denotes the time at which $r(t)$ reaches its maximum. It is assumed here that the pulse width is shorter than the critical pulse width t_p^* [18]. Thus, the depolarization factor lies at the end of the pulse as shown in Fig. 2, i.e.,

$$t^* = t_p, \text{ for } t_p \leq t_p^*. \tag{9}$$

There are two unknown parameters g and τ on the right side of (8). Thus, it is required to acquire at least two IO curves at different pulse widths to estimate τ and g. Since stimulation at two pulse widths is in principle sufficient for the estimation of these parameters, this paper focuses on two IO curves. In this case, Eq. (8) is re-written as

$$\theta_{3_i} = \frac{\alpha\tau^2 - 2\sigma\tau + 1}{k_1} \times \frac{1}{-\omega e^{-t_{p_i}/\tau} + \Big((\alpha\tau - \sigma)\sin\omega t_{p_i} + \omega\cos\omega t_{p_i}\Big)e^{-\sigma t_{p_i}}}, \tag{10}$$

where θ_{3_i} and t_{p_i} are the mid point and pulse width of the $i-$th IO curve with $i = 1,\ 2$.

The membrane time constant τ is obtained by solving $\theta_{3_1}/\theta_{3_2}$ as follows:

$$\frac{\theta_{3_1}}{\theta_{3_2}} = \frac{-\omega e^{-t_{p_2}/\tau} + \Big((\alpha\tau - \sigma)\sin\omega t_{p_2} + \omega\cos\omega t_{p_2}\Big)e^{-\sigma t_{p_2}}}{-\omega e^{-t_{p_1}/\tau} + \Big((\alpha\tau - \sigma)\sin\omega t_{p_1} + \omega\cos\omega t_{p_1}\Big)e^{-\sigma t_{p_1}}} \tag{11}$$

After the estimation of τ, the gain g is then computed by solving (10) for $i = 1$ or 2.

5. Sequential parameter estimation

As discussed earlier, at least two IO curves with different pulse widths t_{p_1} and t_{p_2} are required. Denote the parameter vectors of the first and second IO curves separately as

$$\boldsymbol{\theta}_1 = [\ \theta_{1_1} \quad \theta_{2_1} \quad \theta_{3_1} \quad \theta_{4_1}\ ] \text{ and} \tag{12}$$

$$\boldsymbol{\theta}_2 = [\ \theta_{1_2} \quad \theta_{2_2} \quad \theta_{3_2} \quad \theta_{4_2}\ ]. \tag{13}$$

The sequential parameter estimation starts by taking samples from the baseline.

Subsequently, the pulse width of the cTMS device is set to t_{p_1}, three initial pulse amplitudes are chosen randomly between $V_C(\min)$ and $V_C(\max)$, and the corresponding MEPs are measured. Then, the pulse width of the cTMS device is set to t_{p_2}, three initial pulse amplitudes are chosen randomly between $V_C(\min)$ and $V_C(\max)$, and the corresponding MEPs are measured. The initial stimuli can be performed at the same pulse amplitudes for both pulse widths.

In the next step, initial estimations of $\boldsymbol{\theta}_1$ and $\boldsymbol{\theta}_2$ are obtained by fitting the sigmoid model (7) to the baseline and initial stimuli-response data. The membrane time constant and gain g are then computed by using the estimated θ_{3_1} and θ_{3_2} as described in the previous section.

The next pulse amplitudes, $V_{C_1,n+1}$ for IO curve estimation with pulse width t_{p_1} and $V_{C_2,n+1}$ for IO curve estimation with pulse width t_{p_2}, are computed and administered by solving the FIM optimization problem

$$\begin{aligned} \underset{V_{C_i,n+1}}{\text{minimize}} \quad & -\det\Big(\tilde{\mathbf{F}}_{i,n+1}(V_{C_i,n+1}, \hat{\boldsymbol{\theta}}_{i,n})\Big) \\ \text{subject to} \quad & V_C(\min) \leq V_{C_i,n+1} \leq V_C(\max) \\ \text{for} \quad & i = 1, 2, \text{ and } n \geq 3. \end{aligned} \tag{14}$$

where $\tilde{\mathbf{F}}_{i,n+1}$ is the FIM of the $i-$th IO curve at the $(n+1)-$th stimulus, and $\hat{\boldsymbol{\theta}}_{i,n}$ is the estimate of the $i-$th IO curve's parameter vector at the $n-$th stimulus. Details of such optimization have been discussed previously [49].

The MEP characteristics are measured, and the data sets are updated for both IO curves. The estimations of $\boldsymbol{\theta}_1$ and $\boldsymbol{\theta}_2$ are updated by fitting the sigmoid model (7) to the baseline and updated stimuli-response data. The estimation of τ and g are then updated by using the most recent estimates of θ_{3_1} and θ_{3_2} as described in the previous section. This process is continued until the convergence criterion

$$\left|\frac{\hat{z}_n - \hat{z}_{n-1}}{\hat{z}_{n-1}}\right| < \epsilon_z \tag{15}$$

is satisfied for T consecutive times, $T \geq 1$, for all parameters $z = \{\theta_{j_i},\ \tau,\ g\}$, $j = 1, \ldots, 4,\ i = 1,\ 2$. $\hat{z}_n$ denotes the estimate of z after the $n-$th stimulus. ϵ_z denotes the convergence tolerance. The estimation accuracy is adjustable by ϵ_z and T values. The larger the T value and the smaller the ϵ_z values, the more the accurate estimation is obtained at the cost of more pulses, [49].

6. Simulation Results

The effectiveness of the proposed sequential parameter estimation method is evaluated through 73 simulation runs in Matlab R2021a (The MathWorks, Inc.).

In each run, a true membrane dynamics $h(t)$ is generated with the time constant randomly chosen between 90 and 220 µs. The critical pulse width is obtained by using the following equation [53]:

$$t_p^* = 97.54e^{1206\tau} - 80.57e^{-25000\tau} \tag{16}$$

Two pulse widths t_{p_1} and t_{p_2} are randomly selected between 10 µs and t_p^*. If no prior approximate information about the neural membrane time constant is available, it is suggested to choose short pulse widths.

By randomly choosing g between 30 and 50, the true values of the IO curve's mid points θ_{3_1} and θ_{3_2} are computed, which are real scalars between 0 and 1. Without loss of generality, the lower and upper plateaus are assumed to be the same for both IO curves, i.e., $y^1 = \theta_{1_i}$, and $y^h = \theta_{2_i}$, $i = 1, 2$. The true value of y^l is randomly chosen between –6.5 and –5.5 (corresponding to 0.32 and 3.2 μV), and the true value of y^h is randomly selected between –3 and –2 (corresponding to 1 and 10 mV). True values of the slopes, θ_{4_1} and θ_{4_2}, are randomly chosen between 1 and 100. The reference IO curves are generated by using these random data for all 73 runs. The stimulus–response pairs are generated by applying Gaussian noise with standard deviations of 0.05 and 0.1 to the x and y axes, respectively [54, 55].

The problem in this section is to concurrently estimate the true values of the membrane time constant, coupling factor, and IO curves' parameters by using the proposed sequential parameter estimation (SPE) method.

Fifty baseline samples are arbitrarily taken for all IO curves in all runs.

Every time the estimation of the IO curves and parameter vectors is updated, the trust-region curve fitting algorithm is run with lower and upper limits on the parameter vector as follows:

$$\begin{aligned}
&\boldsymbol{\theta}_i(\min) = [-7 \quad -3 \quad 0 \quad 1] \\
&\boldsymbol{\theta}_i(\max) = [-5 \quad -2 \quad 1 \quad 100] \\
&i = 1,\ 2
\end{aligned}$$

The curve fitting is performed on the logarithmic scale to mitigate the highly skewed variabilities' effects [17, 10]. A bad-fit detection and removal technique is used to avoid sudden estimation jumps.

The estimation of the time constant is updated by solving (11) using fmincon and the global search interior-point algorithm with a random initial guesses, and minimum and maximum limits of 90 µs and 220 µs, respectively.

The optimization problem (14) is solved by using fmincon and the global search interior-point algorithm with a random initial guesses, and minimum and maximum limits of 0.01 and 1, respectively.

For each IO curve, the maximum number of pulses is arbitrarily set to $n_{\max} = 500$, which means that 1000 stimuli can be administered in total.

The stopping rule is based on $T = 5$ successive satisfaction of the the convergence criterion (15) with the tolerance ϵ_z set to 0.01 for all parameters.

6.1. The results of a representative run

Fig. 3 shows the stimulus–response pairs ('×' signs) and reference IO curves (solid lines) for a representative run

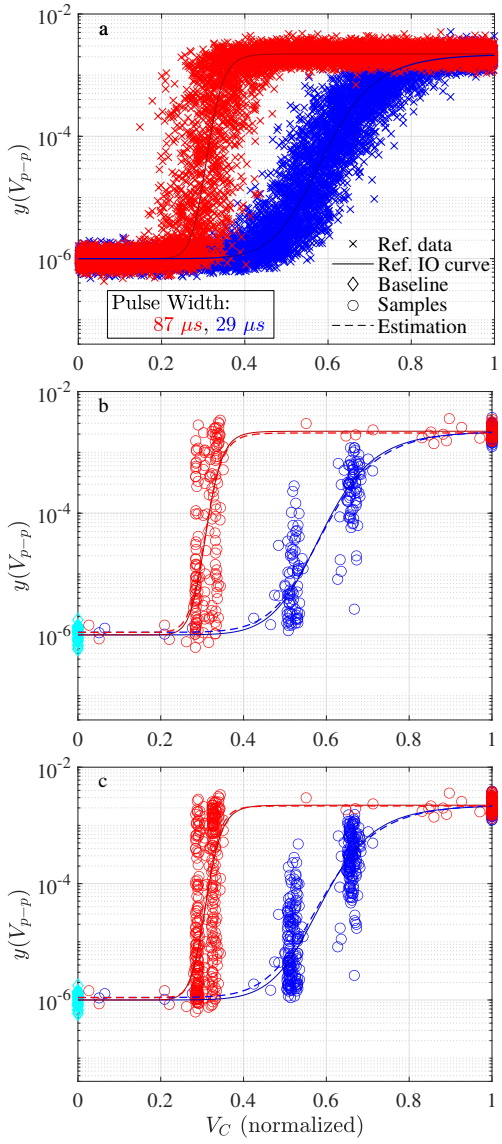

Figure 3: Sample simulation run: (a) reference data and IO curves, estimation by using the proposed method at (b) $n = n_f = 240$ and (c) $n = n_{\max} = 500$.

with the following arbitrarily chosen true values:

$$\begin{aligned}
\tau^{\text{true}} &= 92.05 \text{ µs} \\
g^{\text{true}} &= 32.44 \\
t_{p_1}^{\text{true}} &= 29 \text{ µs} \\
t_{p_2}^{\text{true}} &= 87 \text{ µs} \\
\boldsymbol{\theta}_1^{\text{true}} &= [\ -6.00 \quad -2.65 \quad 0.59 \quad 9.49\ ] \\
\boldsymbol{\theta}_2^{\text{true}} &= [\ -6.00 \quad -2.65 \quad 0.31 \quad 15.97\ ]
\end{aligned}$$

The critical pulse width $t_p^* = 100.93$ µs is obtained by solving by using (16) for $\tau^{\text{true}} = 92.05$ µs. For the formalism simplifications, the pulse widths should be be shorter than t_p^*. The sequential parameter estimation method satisfies the stopping rule at $n = n_f = 240$ for each IO curve, for this representative run. This means that the parame-

ters have been estimated after administering 2×240=480 stimuli.

Fig. 3-b and Fig. 3-c summarize the stimulus–response pairs as well as the estimated IO curves at $n_f = 240$ and $n_{\max}$ for a randomly chosen case. As discussed in [49], it is seen that the FIM optimization administers stimuli, mainly from sectors which contain the maximum information for curve fitting. Fig. 4 shows the conversion behavior of the the IO curves' parameter estimates with increasing number of pulses. Fig. 5 presents the correspondingly estimated time constant and Fig. 6 the estimate of g. The results confirm satisfactory estimation of the membrane time constant τ, g, and the reference IO curves with their parameters.

6.2. The results of 73 runs

All 73 runs satisfied the stopping rule with an average of $n_f = 172$ stimuli for each IO curve, which means that 2×172=344 stimuli were administered in average for the estimation of all parameters and the IO curves.

For all parameters, the absolute relative estimation errors (AREs) after the stimulation of the $n-$th stimulus for each IO curve are computed per

$$e = \left| \frac{\hat{z}_n - z^{\text{true}}}{z^{\text{true}}} \right|, \tag{17}$$

where $z = \{\theta_{j_i},\ \tau,\ g\}$, $j = 1, \ldots, 4,\ i = 1,\ 2$; $\hat{z}_n$ denotes the estimation of z after $n-$th stimulus.

When the stopping rule is satisfied, the IO curves' parameters θ_1, θ_2, θ_3, and θ_4 are estimated with average AREs of 0.2%, 0.7%, 0.9%, and 14.5%, respectively. The membrane time constant τ and gain g are estimated with average AREs of 6.2% and 5.3%, respectively.

At $n = n_{\max} = 500$, the IO curves' parameters θ_1, θ_2, θ_3, and θ_4 are estimated with average AREs of 0.2%, 0.4%, 0.6%, and 8.7%, respectively. The membrane time constant τ and gain g are estimated with average AREs of 5.2% and 4.3%, respectively, at $n = n_{\max}$.

It is noted that the estimation performance of at $n = n_f$ could be improved further by reducing the convergence tolerance ϵ_z or by increasing the number of successive times the convergence criteria must be satisfied.

7. Conclusions and future works

TMS devices with adjustable pulse duration, such as cTMS, allow closed-loop sequential parameter estimation of the linearized neural membrane time constant, the input–output (IO) curve, as well as coupling and scaling gains. Stimulation at two pulse widths is in principle sufficient for the estimation of these parameters in electromyography-guided (EMG-guided) TMS. The proposed two-stage sequential parameter estimation method demonstrates satisfactory estimation performance over 70 simulation case studies with around 5% average absolute relative estimation error (ARE) for 500 pulses.

References

[1] Polson MJ, Barker AT, Freeston IL. Stimulation of nerve trunks with time-varying magnetic fields. Medical & biological engineering & computing 1982; 20(2):243–244.

[2] Barker AT, Jalinous R, Freeston IL. Non-invasive magnetic stimulation of human motor cortex. The Lancet 1985; 325(8437):1106–1107.

[3] Ziemann U. Thirty years of transcranial magnetic stimulation: where do we stand? Experimental Brain Research 2017; 235:973-–984.

[4] Valero-Cabré A, Amengual JL, Stengel C, Pascual-Leone A, and Coubard OA, Transcranial magnetic stimulation in basic and clinical neuroscience: A comprehensive review of fundamental principles and novel insights. Neuroscience & Biobehavioral Reviews 2017; 83:381–404.

[5] Gomez LJ, Goetz SM, Peterchev AV. Design of transcranial magnetic stimulation coils with optimal trade-off between depth, focality, and energy. Journal of Neural Engineering 2018; 15:046033.

[6] Kammer T, Beck S, Erb M, Grodd W. The influence of current direction on phosphene thresholds evoked by transcranial magnetic stimulation. Clinical Neurophysiology. 2001; 112(11):2015–2021.

[7] Kammer T, Beck S, Thielscher A, Laubis-Herrmann U, Topka H. Motor thresholds in humans: a transcranial magnetic stimulation study comparing different pulse waveforms, current directions and stimulator types. Clinical Neurophysiology. 2001; 112(2):250–258.

[8] Sommer M, Alfaro A, Rummel M, Speck S, Lang N, Tings T, Paulus W. Half sine, monophasic and biphasic transcranial magnetic stimulation of the human motor cortex. Clinical Neurophysiology. 2006; 117(4):838–844.

[9] Goetz SM, Luber B, Lisanby SH, Murphy DLK, Kozyrkov IC, Grill WM, Peterchev AV. Enhancement of neuromodulation with novel pulse shapes generated by controllable pulse parameter transcranial magnetic stimulation. Brain Stimulation. 2016; 9(1):39–47.

[10] D'Ostilio K, Goetz SM, Hannah R, Ciocca M, Chieffo R, Chen J-C A, Peterchev AV, Rothwell JC. Effect of coil orientation on strength–duration time constant and I-wave activation with controllable pulse parameter transcranial magnetic stimulation. Clinical Neurophysiology 2016; 127:675–683.

[11] Sommer M, Ciocca M, Chieffo R, Hammond P, Neef A, Paulus W, Rothwell JC, Hannah R. TMS of primary motor cortex with a biphasic pulse activates two independent sets of excitable neurones. Brain Stimulation. 2018; 11(3):558–565.

[12] Halawa I, Shirota Y, Neef A, Sommer M, Paulus W. Neuronal tuning: selective targeting of neuronal populations via manipulation of pulse width and directionality. Brain Stimulation. 2019; 12(5):1244–1252.

[13] Hannah R, Rothwell JC. Pulse Duration as Well as Current Direction Determines the Specificity of Transcranial Magnetic Stimulation of Motor Cortex during Contraction. Brain Stimulation 2017; 10:106—115.

[14] Barker AT, Garnham CW, Freeston IL. Magnetic nerve stimulation: the effect of waveform on efficiency, determination of neural membrane time constants and the measurement of stimulator output. Electroencephalogr Clin Neurophysiol Suppl 1991; 43:227—37.

[15] Corthout E, Barker AT, Cowey A. Transcranial magnetic stimulation. Which part of the current waveform causes the stimulation? Exp Brain Res 2001; 141:128-–32.

[16] Amassian VE, Maccabee PJ. Transcranial Magnetic Stimulation. International Conference of the IEEE Engineering in Medicine and Biology Society (EMBS) 2006; 22:1620-1623. doi: 10.1109/IEMBS.2006.259398.

[17] Peterchev AV, Goetz SM, Westin GG, Luber B, Lisanby SH. Pulse width dependence of motor threshold and input–output curve characterized with controllable pulse parameter transcranial magnetic stimulation. Clinical Neurophysiology 2013; 124:1364–1372.

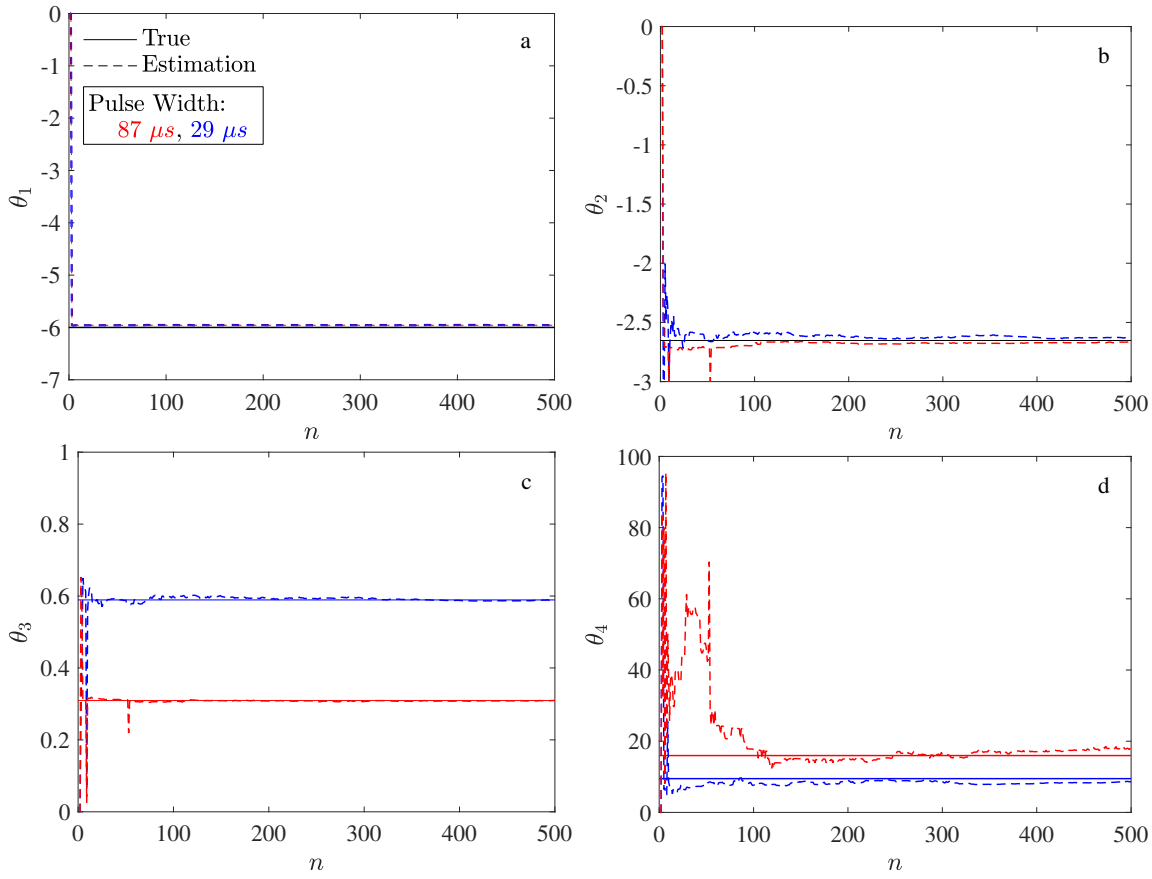

Figure 4: Estimation of the IO curves parameters.

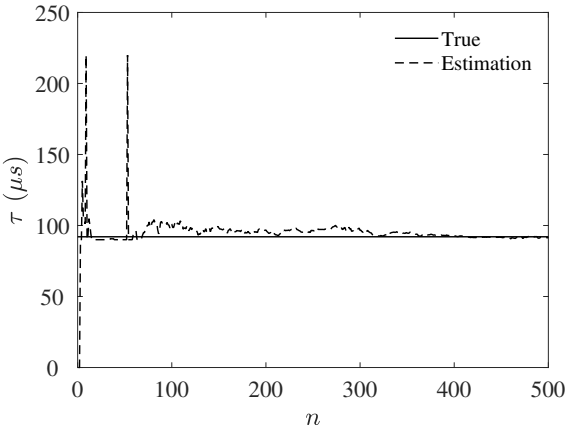

Figure 5: Estimation of the membrane time constant τ.

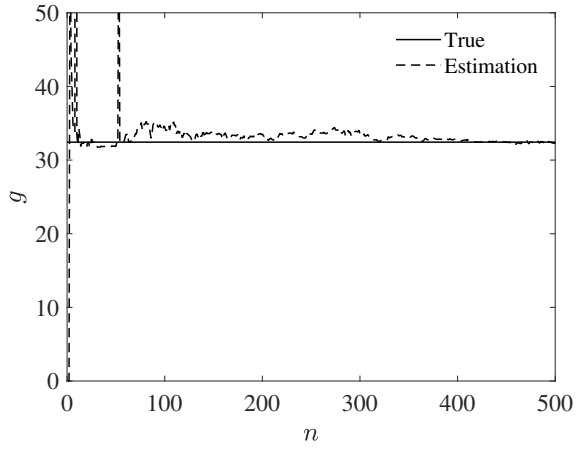

Figure 6: Estimation of the coupling factor g.

[18] Alavi SMM, Vila-Rodriguez F, Mahdi A, Goetz SM. Sequential estimation of neural membrane time-constant and input-output curve towards selective and closed-loop transcranial magnetic stimulation. bioRxiv Preprint 2022. DOI: https://doi.org/10.1101/2022.04.05.487065

[19] Rattay F, Paredes LP, Leao RN. Strength–duration relationship for intra- versus extracellular stimulation with microelectrodes. Neuroscience 2012; 214:1–13.

[20] Mogyoros I, Kiernan MC, Burke D. Strength-duration properties of human peripheral nerve. Brain 1996; 119 (Pt 2):439-47.

[21] Geddes LA. Accuracy limitations of chronaxie values. IEEE Trans Biomed Eng. 2004; 51:176–181.

[22] Yerdelen D, Koc F, Uysal H. Strength–duration properties of sensory and motor axons in alcoholic polyneuropathy. Neurological Research 2008; 30(7): 746-750.

[23] Boinagrov D, Loudin J, Palanker D. Strength–duration relationship for extracellular neural stimulation: numerical and analytical models. J Neurophysiol. 2010; 104:2236–2248.

[24] Farrar MA, Vucic S, Lin CS, Park SB, Johnston HM, du Sart D, et al. Dysfunction of axonal membrane conductances in adolescents and young adults with spinal muscular atrophy. Brain. 2011; 134:3185–3197.

[25] Lin CS, Krishnan AV, Park SB, Kiernan MC. Modulatory

effects on axonal function after intravenous immunoglobulin therapy in chronic inflammatory demyelinating polyneuropathy. Arch Neurol. 2011; 68:862–869.

[26] Moldovan M, Alvarez S, Pinchenko V, Marklund S, Graffmo KS, Krarup C. Nerve excitability changes related to axonal degeneration in amyotrophic lateral sclerosis: Insights from the transgenic SOD1(G127X) mouse model. Exp Neurol. 2012; 233:408–420.

[27] Lugg A, Schindle M, Sivak A, Tankisi H, Jones KE. Nerve excitability as a biomarker for amyotrophic lateral sclerosis: a systematic review and meta-analysis. medRxiv 2022; doi: https://doi.org/10.1101/2022.02.11.22270866

[28] Rossini PM. Methodological and physiological aspects of motor evoked potentials. Electroencephalography and Clinical Neurophysiology Suppl. 1990; 41:124–133.

[29] Ghaly RF, Stone JL, Aldrete JA, and Kartha RK. Transcranial magnetic induced motor evoked potentials in primates: the technique and anesthetic effects. Images of the Twenty-First Century. IEEE Proceedings of the Annual International Engineering in Medicine and Biology Society, 1989; 1573-1574.

[30] Klomjai W, Katz R, Lackmy-Vallée. Basic principles of transcranial magnetic stimulation (TMS) and repetitive TMS (rTMS). Annals of Physical and Rehabilitation Medicine 2015; 58(4):208–213.

[31] Westin GG, Bassi BD, Lisanby SH, Luber B. Determination of motor threshold using visual observation overestimates transcranial magnetic stimulation dosage: safety implications. Clinical Neurophysiology 2014; 125(1):142–147.

[32] Li Z, Peterchev AV, Rothwell JC, Goetz SM. Detection of Motor-Evoked Potentials Below the Noise Floor: Rethinking the Motor Threshold. bioRxiv 2021.12.10.472126. doi: 10.1101/2021.12.10.472126

[33] Goetz SM, Li Z, Peterchev AV. Noninvasive detection of motor-evoked potentials in response to brain stimulation below the noise floor—how weak can a stimulus be and still stimulate. Proc IEEE Eng Med Biol Soc (EMBC) 2018; 40:2687–2690. doi: 10.1109/EMBC.2018.8512765

[34] Goetz SM and Deng ZD. The development and modelling of devices and paradigms for transcranial magnetic stimulation. International Review of Psychiatry 2017; 29(2):115–145.

[35] Peterchev AV, Jalinous R, Lisanby SH. A Transcranial Magnetic Stimulator Inducing Near-Rectangular Pulses With Controllable Pulse Width (cTMS). IEEE Trans Biomed Eng 2008;55(1):257–66.

[36] Goetz SM, Pfaeffl M, Huber J, Singer M, Marquardt R, Weyh T. Circuit topology and control principle for a first magnetic stimulator with fully controllable waveform. Proc IEEE Eng Med Biol Soc (EMBC) 2012; 34:4700–4703. doi: 10.1109/EMBC.2012.6347016

[37] Li Z, Zhang J, Peterchev AV, Goetz SM. Modular Pulse Synthesizer for Transcranial Magnetic Stimulation with Flexible User-Defined Pulse Shaping and Rapidly Changing Pulses in Sequences. 2022; arXiv:2202.06530. doi: 10.48550/ARXIV.2202.06530

[38] Zeng Z, Koponen LM, Hamdan R, Li Z, Goetz SM, Peterchev AV. Modular multilevel TMS device with wide output range and ultrabrief pulse capability for sound reduction. Journal of Neural Engineering. 2022; 19(2):026008.

[39] Polson MJR. Magnetic stimulator for neuro-muscular tissue. US Patent and Trademark Office 1998; US 5,766,124.

[40] Karabanov A, Thielscher A, Siebner HR. Transcranial brain stimulation: Closing the loop between brain and stimulation. Curr Opin Neurol 2016;29(4):397-–404.

[41] Tervo AE, Nieminen JO, Lioumis P, Metsomaa J, Souza VH, Sinisalo H, Stenroos M, Sarvas J, Ilmoniemia RJ. Closed-loop optimization of transcranial magnetic stimulation with electroencephalography feedback, Brain Stimulation 2021; 14:P1674.

[42] Wang B, Peterchev AV, and Goetz SM. Analysis and Comparison of Methods for Determining Transcranial Magnetic Stimulation Thresholds. bioRxiv 2022; 495134v1. doi: 10.1101/2022.06.26.495134

[43] Treutwein B and Strasburger H. Fitting the psychometric function. Perception & Psychophysics 1999; 61(1):87–106.

[44] Awiszus F. Fast estimation of transcranial magnetic stimulation motor threshold: is it safe?. Brain Stimulation: Basic, Translational, and Clinical Research in Neuromodulation 2011; 4(1):58–59.

[45] Bergmann TO, Mölle M, Schmidt MA, Lindner C, Marshall L, Born J, Siebner HR. EEG-guided transcranial magnetic stimulation reveals rapid shifts in motor cortical excitability during the human sleep slow oscillation. Journal of Neuroscience 2012; 32(1):243–53.

[46] Zrenner C, Desideri D, Belardinelli P, Ziemann U. Real-time EEG-defined excitability states determine efficacy of TMS-induced plasticity in human motor cortex, Brain Stimulation 2018; 11(2):374–389.

[47] Ding Z, Ouyang G, Chen H, Li X. Closed-loop transcranial magnetic stimulation of real-time EEG based on the AR mode method. Biomed. Phys. Eng. Express 2020; 6:035010.

[48] Pankka H, Roine T, Lehtinen J, Ilmoniemi, RJ. Improving closed-loop TMS timing using the Wavenet model. Brain Stimulation 2021; 14(6):P1636–1637.

[49] Alavi SMM, Goetz SM, Peterchev AV. Optimal estimation of neural recruitment curves using Fisher information: application to transcranial magnetic stimulation. IEEE Transactions on Neural Systems and Rehabilitation Engineering 2019; 27:1320–1330.

[50] Alavi SMM, Goetz SM, Saif M. Input-Output Slope Curve Estimation in Neural Stimulation Based on Optimal Sampling Principles. Journal of Neural Engineering 2021; 18:046071.

[51] Goetz SM, Weyh T, Afinowi IAA, Herzog HG. Coil Design for Neuromuscular Magnetic Stimulation Based on a Detailed 3-D Thigh Model. IEEE Transactions on Magnetics 2014; 50(6):1–10.

[52] Aberra AS, Peterchev AV, and Grill WM. Biophysically realistic neuron models for simulation of cortical stimulation. Journal of Neural Engineering 2018; 15(6):066023.

[53] Alavi SMM, Vila-Rodriguez F, Mahdi A, Goetz SM. Closed-loop and automatic tuning of pulse amplitude and width in EMG-guided controllable transcranial magnetic stimulation (cTMS). bioRxiv preprint 2022. doi: 10.1101/2022.05.08.491097

[54] Goetz SM, Luber B, Lisanby SH, Peterchev AV. A Novel Model Incorporating Two Variability Sources for Describing Motor Evoked Potentials. Brain Stimulation 2014; 7:541–552.

[55] Goetz SM, Alavi SMM, Deng Z-D, Peterchev AV. Statistical Model of Motor Evoked Potentials. IEEE Transactions on Neural Systems and Rehabilitation Engineering 2019; 27:1539–1545.

[56] Aberra AS, Peterchev AV, Grill WM. Biophysically realistic neuron models for simulation of cortical stimulation. Journal of neural engineering. 2018; 15(6):066023.